Hybrid III-V/SOI resonant cavity enhanced photodetector

Learkthanakhachon, Supannee; Taghizadeh, Alireza; Park, Gyeong Cheol; Yvind, Kresten; Chung, Il-Sug

Published in:
Optics Express

Link to article, DOI:
10.1364/OE.24.016512

Publication date:
2016

Document Version
Publisher's PDF, also known as Version of record

Research Article | Vol. 24, No. 15 | 25 Jul 2016 | OPTICS EXPRESS 16512

Optics EXPRESS

Hybrid III-V/SOI resonant cavity enhanced photodetector

SUPANNEE LEARKTHANAKHACHON, ALIREZA TAGHIZADEH, GYEONG CHEOL PARK, KRESTEN YVIND, AND IL-SUG CHUNG*

Department of Photonics Engineering (DTU Fotonik), Technical University of Denmark Ørsteds Plads, DK-2800 Kgs. Lyngby, Denmark
ilch@fotonik.dtu.dk

Abstract: A hybrid III-V/SOI resonant-cavity-enhanced photodetector (RCE-PD) structure comprising a high-contrast grating (HCG) reflector, a hybrid grating (HG) reflector, and an air cavity between them, has been proposed and investigated. In the proposed structure, a light absorbing material is integrated as part of the HG reflector, enabling a very compact vertical cavity. Numerical investigations show that a quantum efficiency close to 100 % and a detection linewidth of about 1 nm can be achieved, which are desirable for wavelength division multiplexing applications. Based on these results, a hybrid RCE-PD sample has been fabricated by heterogeneously integrating an InP-based material onto a silicon-on-insulator wafer and has been characterized, which shows a clear enhancement in photo-current at the designed wavelength. This indicates that the HG reflector provides a field enhancement sufficient for RCE-PD operation. In addition, a capability of feasibly selecting the detection wavelength during fabrication as well as a possibility of realizing silicon-integrated bi-directional transceivers are discussed.

OCIS codes: (040.5160) Photodetectors; (050.2770) Gratings; (050.6624) Subwavelength structures; (060.4230) Multiplexing; (250.3140) Integrated optoelectronic circuits; (250.0040) Detectors.

References and links

1. C. Mateus, M. Huang, L. Chen, C. Chang-Hasnain, and Y. Suzuki, "Broad-band mirror (1.12-1.62 μm) using a subwavelength grating," IEEE Photon. Technol. Lett. **16**, 1676–1678 (2004).
2. D. Fattal, J. Li, Z. Peng, M. Fiorentino, and R. G. Beausoleil, "Flat dielectric grating reflectors with focusing abilities," Nat. Photonics **4**, 466–470 (2010).
3. F. Lu, F. G. Sedgwick, V. Karagodsky, C. Chase, and C. J. Chang-Hasnain, "Planar high-numerical-aperture low-loss focusing reflectors and lenses using subwavelength high contrast gratings," Opt. Express **18**, 12606–12614 (2010).
4. L. Carletti, R. Malureanu, J. Mørk, and I.-S. Chung, "High-index-contrast grating reflector with beam steering ability for the transmitted beam," Opt. Express **19**, 23567–23572 (2011).
5. C. Sciancalepore, B. B. Bakir, X. Letartre, J.-M. Fedeli, N. Olivier, D. Bordel, C. Seassal, P. Rojo-Romeo, P. Regreny, and P. Viktorovitch, "Quasi-3D light confinement in double photonic crystal reflectors VCSELs for CMOS-compatible integration," J. Lightwave Technol. **29**, 2015–2024 (2011).
6. M. C. Huang, Z. Y., and C. J. Chang-Hasnain, "A surface-emitting laser incorporating a high-index-contrast subwavelength grating," Nat. Photonics **1**, 119–122 (2007).
7. I.-S.Chung, J. Mørk, P. Gilet, and A. Chelnokov, "Subwavelength grating-mirror VCSEL with a thin oxide gap," IEEE Photon. Technol. Lett. **20**, 105–107 (2008).
8. M. C. Y. Huang, Y. Zhou, and C. J. Chang-Hasnain, "A nanoelectromechanical tunable laser," Nat. Photonics **2**, 180–184 (2008).
9. I.-S. Chung, V. Iakovlev, A. Sirbu, A. Mereuta, A. Caliman, E. Kapon, and J. Mørk, "Broadband MEMS- tunable high-index-contrast subwavelength grating long-wavelength VCSEL," IEEE J. Quantum Electron. **46**, 1245–1253 (2010).
10. T. Ansbæk, I.-S. Chung, E. S. Semenova, O. Hansen, and K. Yvind, "Resonant MEMS tunable VCSEL," IEEE J. Sel. Top. Quantum Electron. **19**, 1702306–1702311 (2013).
11. I.-S. Chung and J. Mørk, "Silicon-photonics light source realized by III-V/Si-grating-mirror laser," Appl. Phys. Lett. **97**, 151113 (2010).
12. P. Viktorovitch, C. Sciancalepore, B. B. Bakir, X. Letartre, and C. Seassal, "Double photonic crystal vertical-cavity surface-emitting lasers," Proc. SPIE **8633**, 863302 (2013).
13. G. C. Park, W. Xue, A. Taghizadeh, E. Semenova, K. Yvind, J. Mørk, and I.-S. Chung, "Hybrid vertical-cavity laser with lateral emission into a silicon waveguide," Laser Photon. Rev. **9**, L11 (2015).

#267167 http://dx.doi.org/10.1364/OE.24.016512
Journal © 2016 Received 26 May 2016; revised 2 Jul 2016; accepted 3 Jul 2016; published 13 Jul 2016

Optics EXPRESS

14. G. C. Park, W. Xue, E. Semenova, Jesper Mørk, and I.-S.Chung, "III-V/SOI vertical cavity laser structure for 120 Gbit/s speed," in *Advanced Photonics*, JT5A (post-deadline) (Optical Society of America, Boston, 2015), p. JT5A.2.
15. B. Zhang, Z. Wang, S. Brodbeck, C. Schneider, M. Kamp, S. Höfling, and H. Deng, "Zero-dimensional polariton laser in a subwavelength grating-based vertical microcavity," Light Sci. Appl. **3**, e135 (2014).
16. Z. Wang, B. Zhang, and H. Deng, "Dispersion engineering for vertical microcavities using subwavelength gratings," Phys. Rev. Lett. **114**, 073601 (2015).
17. A. Taghizadeh, J. Mørk, and I.-S. Chung, "Vertical-cavity in-plane heterostructures: Physics and applications," Appl. Phys. Lett. **107**, 181107 (2015).
18. I.-S. Chung, A. M. V. Iakovlev, A. Caliman, A. Syrbu, E. Kapon, and J. Mørk, "Selectively-pumped graiting-mirror long wavelength VCSEL," in *Proceedings of IEEE International Conference on Indium Phosphide and Related Materials* (Institute of Electrical and Electronics Engineerings, 2009). p. 403.
19. I.-S.Chung, "Study on differences between high contrast grating reflectorsfor TM and TE polarizations and their impact on VCSEL designs," Opt. Express **23**, 16730–16739 (2015).
20. J. Ferrara, W. Yang, L. Zhu, P. Qiao, and C. J. Chang-Hasnain, "Heterogeneously integrated long-wavelength VCSEL using silicon high contrast grating on an SOI substrate," Opt. Express **23**, 2512–2523 (2015).
21. A.Taghizadeh, G.C.Park, J. Mørk, and I.-S. Chung, "Hybrid grating reflector with high reflectivity and broad bandwidth," Opt. Express **22**, 21175–21184 (2014).
22. G. C. Park, A. Taghizadeh, and I.-S. Chung, "Hybrid grating reflectors: Origin of ultrabroad stopband," Appl. Phys. Lett. **108**, 141108 (2016).
23. A. Taghizadeh, J. Mørk, , and I.-S. Chung, "Ultracompact resonator with high quality-factor based on a hybrid grating structure," Opt. Express **23**, 14913–14921 (2015).
24. R. Magnusson, "Wideband reflectors with zero-contrast gratings," Opt. Lett. **39**, 4337–4340 (2014).
25. V. Topić and I.-S. Chung, "Comparative study of heat dissipation capabilities of hybrid III-V/SOI vertical cavity lasers," submitted to IEEE Photon. Technol. Lett.
26. W. Yang, S. A. Gerke, L. Zhu, C. Chase, Y. Rao, and C. J. Chang-Hasnain, "Long-wavelength tunable detector using high-contrast grating," IEEE J. Sel. Topics Quantum Electron. **16**, 3803208 (2014).
27. M. S. Uünlü and S. Strite, "Resonant cavity enhanced photonic devices," Appl. Phys. Rev. **78**, 607–639 (1995).
28. M. G. Moharam, T. K. Gaylord, E. B. Grann, and D. A. Pommet, "Formulation for stable and efficient implementation of the rigorous coupled-wave analysis of binary gratings," J. Opt. Soc. Am. A **12**, 1068–1076 (1995).
29. L. Li, "Use of Fourier series in the analysis of discontinuous periodic structures," J. Opt. Soc. Am. A **13**, 1870–1876 (1996).
30. L. A. Coldren, S. W. Corzine, and M. L. Mašanović, *Diode Lasers and Photonic Integrated Circuits*, 2nd ed. (Wiley, 2012).
31. J. Piprek, *Semiconductor Optoelectronic Devices* (Academic Press, 2003).
32. J. T. Verdeyen, *Laser Electronics* (PrenticeHall, 2000).
33. Y. Zhou, M. C. Y. Huang, and C. J. Chang-Hasnain, "Large fabrication tolerance for VCSELs using high-contrast grating," IEEE Photon. Technol. Lett. **20**, 434–436 (2008).
34. G. P. Agrawal, *Fiber-Optic Communication Systems*, 3rd ed. (Wiley, 2002).
35. I.-S. Chung, Y. T. Lee, J.-E. Kim, and H. Y. Park, "A method to tune the cavity-mode wavelength of resonant cavity-enhanced photodetectors for bidirectional optical interconnects," IEEE Photon. Technol. Lett. **18**, 46–48 (2006).

1. Introduction

The high contrast grating (HCG) is a near-subwavelength grating surrounded by low-refractive-index materials. It can provide a reflectivity close to 100 % over a broad wavelength range [1], as well as control over reflection phase [2–5]. Based on these properties, many interesting vertical-cavity laser (VCL) structures with novel functionalities have been realized [6–18]. Among them, the hybrid VCL approach appears promising for long wavelength applications, which combines a III-V material including a gain material with an HCG reflector formed in the silicon (Si) layer of a Si-on-insulator (SOI) wafer [11–14]. The term, *hybrid* represents the heterogeneous integration of a III-V material with Si. The hybrid VCL can output light into a Si waveguide [11–13] and achieve a very high speed [14] by using an HCG for transverse magnetic (TM) polarization to achieve a very small mode volume [19]. For example, its modulation current efficiency factor can be three-times larger than those of conventional vertical-cavity surface-emitting lasers (VCSELs). These properties make the hybrid VCL a promising candidate light source for chip-level optical interconnect applications as well as large datacenter applications.

Optics EXPRESS

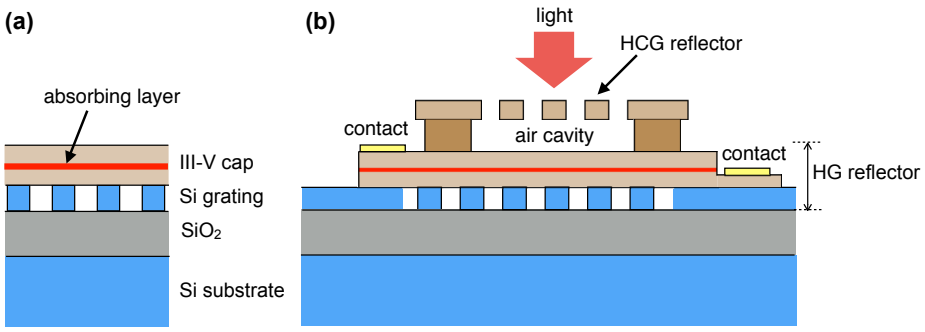

Fig. 1. (a) Schematic cross-section of a III-V/SOI RCE-PD based on an HCG and an HG reflector. (b) Schematic cross-section of an HG reflector with an absorbing layer included in the III-V cap layer.

However, its heat dissipation efficiency is limited by the low-refractive-index material (poor thermal conductor) between the III-V material and the Si HCG, unless a metallic structure is used as a heat spreading channel [11,20]. A recently-reported grating structure referred to *hybrid grating* (HG) [21–23] or *zero-contrast grating* [24] has a potential to solve this challenge.

As shown in Fig. 1(a), the HG structure consists of a Si grating layer and an InP-based layer referred to as *cap layer*. Since HG reflectors can provide an even broader stopband than HCG reflectors [21, 22], a vertical cavity structure comprising an HG reflector with an active material in the cap layer, a dummy cavity, and another mirror can potentially be used for a VCL or a resonant-cavity enhanced photodetector (RCE-PD), as shown in Fig. 1(b). In this cavity, there is no low-refractive-index material between the III-V active layer and the Si grating layer, which facilitates the heat generated around the active layer flowing toward the Si substrate. A comparative investigation of heat dissipation efficiencies of various hybrid VCL structures [25] shows that the main heat dissipation channel is through the Si substrate and the HG-based hybrid VCL structure has a nearly two-times smaller thermal resistance than the HCG-based one, thanks to the increased downward heat flux. Though the HG-based vertical cavity structure has an interesting potential for VCLs or RCE-PDs, there has been no study on whether the field enhancement in the cap layer is strong enough for VCL or RCE-PD operation.

In this paper, we numerically and experimentally investigate a hybrid RCE-PD structure which is based on a HG reflector with an absorbing material in the cap layer. In Section 2, the influence of the absorbing material on the HG reflectance as well as a designing principle for achieving a high absorption efficiency, is discussed based on numerical simulations. In Section 3, a RCE-PD sample is fabricated and characterized. These numerical and experimental results indicate that the field enhancement in the cap layer is sufficiently high for RCE-PD operation. Finally, a capability of determining the detection wavelength during fabrication and a possibility of bi-directional optical transceivers are discussed. This kind of RCE-PDs with a narrow detection bandwidth is highly desirable for wavelength division multiplexing (WDM) application [26], since it can eliminate the need for demultiplexing component, as well as inherently providing a high speed and high responsivity [27].

2. Device structure and design of mirrors

As shown in Fig. 1(b), the hybrid RCE-PD structure consists of an InP HCG, an HG, and an air cavity between them, of which detailed layer structures are presented in Table 1. Numerical investigations used a home-made simulator, which is based on the rigorous coupled wave analysis (RCWA) method [28] and an efficient reformulation for TM polarization [29]. The TM and TE polarizations represent waves with an electric field perpendicular and parallel

Optics EXPRESS

Table 1. Device structure. The III-V cap layer in Fig. 1 is composed of the p-cladding layer to n-cladding layer in this table. The InP HCG has a grating period of 735 nm and a grating bar width of 365 nm, while the Si grating has a period of 735 nm and a bar width of 315 nm.

Layer name	Material	Thickness (nm)	Doping (cm^{-3})
incident medium	air	-	-
HCG layer	InP	530.0	-
gap layer	air	664.0	-
p-cladding layer	InP	380.0	$p = 1 \times 10^{18}$
cladding layer	InP	272.1	-
absorbing layer	InGaAs	12.0	-
cladding layer	InP	97.0	-
etch stop	InGaAsP	5.0	-
n-cladding layer	InP	189.9	$n = 1.5 \times 10^{18}$
grating layer	Si	500.0	-
exiting medium	SiO_2	-	-

to grating bars, respectively. In all simulations, 31 harmonics were used $(= 2 \times 15 + 1)$, which provide good convergence for most of cases. The absorption coefficient for the 12-nm-thick InGaAs absorbing layer was assumed to be a constant value of 5000 cm^{-1}, which is an approximate value for bulk InGaAs at 1.55-μm wavelength [30]. The absorption coefficient for the doped cladding layers, due to the free-carrier absorption was calculated by $\left(25 \times 10^{-18} p + 2 \times 10^{-18} n\right)$, where p and n are p- and n-type doping concentrations in cm^{-3}, respectively [31].

Firstly, let us investigate the effect of absorption in the cap layer on the HG reflectance. Figure 2(a) compares the reflectance spectra of two HGs, which are identical except for the existence of absorption in the cap layer. For the HG with absorption, the reduction in reflectance values occurs over all wavelengths, which is attributed to absorption since there is negligible difference between the transmittance spectra of the two HGs. In the investigated HG structure, the absorption occurs mostly in the InGaAs absorbing layer, while the absorption in the doped cladding layers is found to be negligible. We need to note that the reduction in reflectance is much larger at shorter wavelengths. It appears that if light stays in the HG structure for a longer time, it has more chance of passing the absorbing layers, increasing the amount of absorption. The time for a light staying in the HG structure can be quantified by the reflection delay time, $\tau = (\partial\theta/\partial\lambda) \times (\lambda^2/2\pi c)$ [9], where θ is the reflection phase of the HG reflector and c is the speed of light in the air. As shown in Fig. 2(b), the delay time of the HG is much longer at shorter wavelengths, supporting the explanation above. The HG reflectance, R_{HG} at a target wavelength, λ_0 of 1550 nm is 98.75%, which is denoted by a green dotted line in Fig. 2(a). This value can be adjusted by changing the reflectance of a passive HG (with absorption turned off) or by changing the absorbing layer thickness or absorbing material. The TE reflectance at 1550-nm wavelength is 46.4 %.

In conventional RCE-PD structures, the condition for maximizing the absorption efficiency, η which is defined as the ratio of the absorbed power over the incident power and is sometimes referred to as quantum efficiency, is given by $R_1(\lambda_0) = R_2(\lambda_0) e^{-2\alpha_a(\lambda_0) d_a}$ [27]. Here, R_1 and R_2 are the reflectances of the light incident mirror and exit mirror, and α_a and d_a are the absorption coefficient and thickness of the absorbing layer, respectively. Since in the proposed hybrid RCE-PD structure, the damping of the field intensity occurs not in the cavity but in the HG reflector, the above condition is modified as,

$$R_{\mathrm{HCG}}(\lambda_0) = R_{\mathrm{HG}}(\lambda_0, \alpha_a(\lambda_0), d_a). \tag{1}$$

Optics EXPRESS

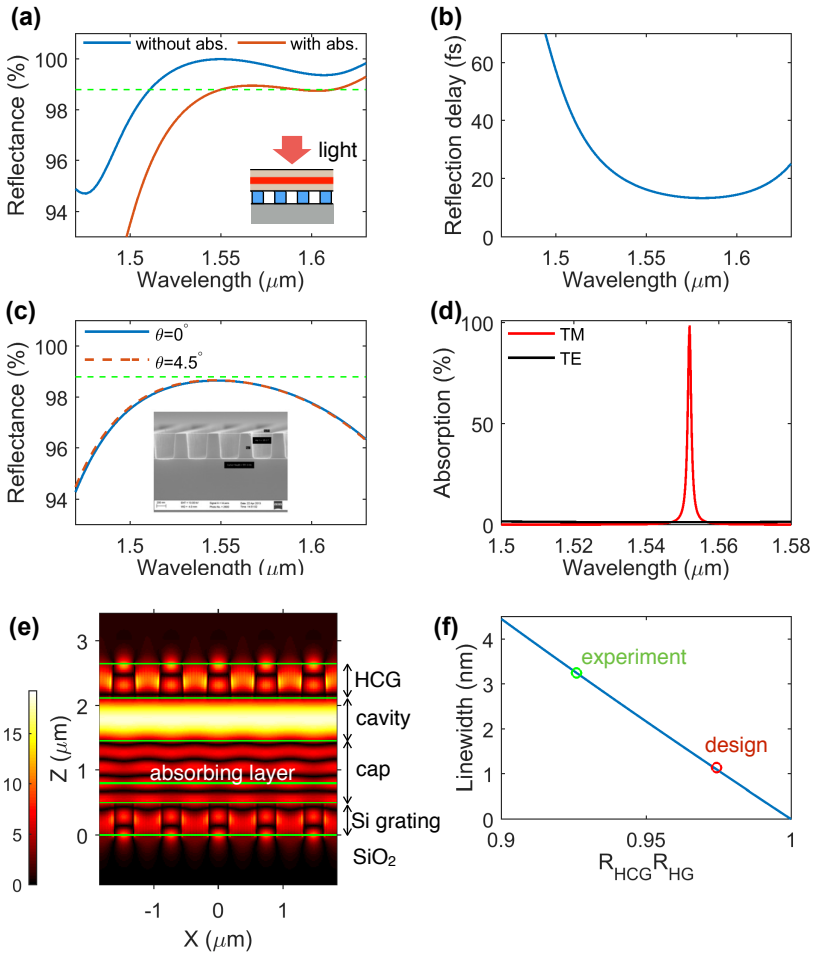

Fig. 2. (a) Calculated reflectance spectra of a HG with and without considering the absorption in the cap layer for TM polarized light. (b) Calculated reflection delay-time spectrum of the HG in (a). (c) Calculated reflectance spectra of HCGs with sidewall angles of 0° and 4.5°, for TM polarized light. (d) Calculated absorption spectra of a RCE-PD for incident fields with different polarizations. (e) Electric field intensity profile, $|E_x|$ at the absorption peak wavelength in (d). (f) Calculated absorption peak linewidth as a function of the product of mirror reflectances.

Here, R_{HCG} and R_{HG} are the reflectances of an HCG and an HG, respectively.

Now, the InP HCG is designed to meet the above condition. From the etching test of InP gratings, it was found that the side wall of grating bars is angled at about 4.5°, as shown in the inset of Fig. 2(c). We have found that in angled cases, if the grating bar width at the middle of the grating height is identical to that of the vertical grating bar (with a zero angle), the angled and vertical cases have almost same reflectance spectra, as shown in Fig. 2(c). Figure 2(c) also shows that at 1550-nm wavelength, the angled HCG reflectance is very close to the HG reflectance value of 98.75 % (green dotted line), satisfying the condition of Eq. (1). The TE reflectance at 1550-nm wavelength is 20.2 %.

As shown in Fig. 2(d), the quantum efficiency of the hybrid RCE-PD with the designed HG and HCG reflectors, reaches close to 100 % at 1550-nm wavelength selectively for a TM polarized incident field. There is no enhancement for TE polarized incident field, since the

Optics EXPRESS

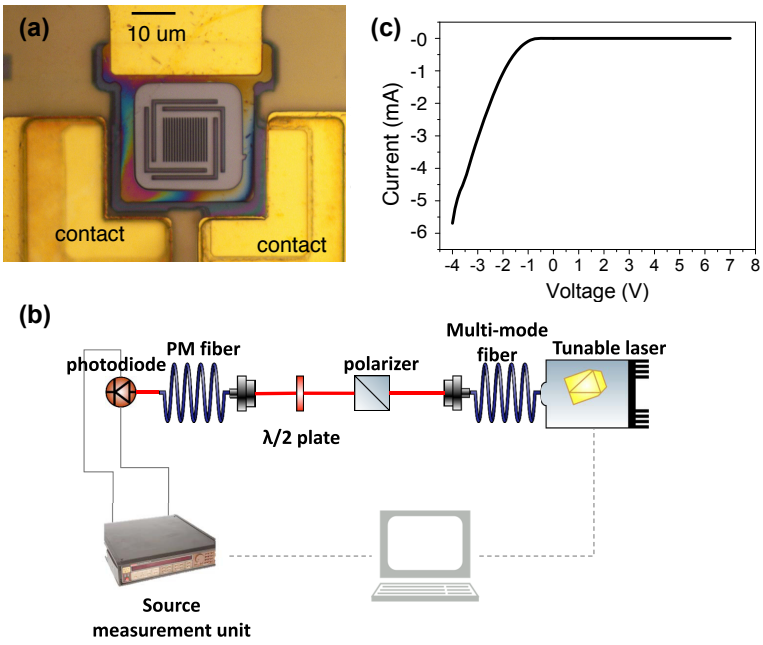

Fig. 3. (a) Optical microscope image of the fabricated sample, seen from the top. (b) Characterization set-up. Red lines represent free-space propagation. (c) Diode characteristic with no incident light.

TE reflectances of both reflectors are not large enough. This shows that though the absorbing layer is not within the cavity, the field enhancement at the intensity maxima in the cap layer is sufficiently high for RCE-PD operation. From theories on resonant optical cavities [32], the full-width half-maximum (FWHM) absorption linewidth, $\Delta\lambda_{1/2}$ can be analytically expressed by $\Delta\lambda_{1/2} = \lambda_0^2/(2\pi d_{\text{eff}})\left(1-(R_{\text{HCG}}R_{\text{HG}})^{1/2}\right)/(R_{\text{HCG}}R_{\text{HG}})^{1/4}$, where d_{eff} is the effective cavity length including the phase penetration depths into the HCG and HG as defined in [9]. In Fig. 2(f), the $\Delta\lambda_{1/2}$ is plotted as a function of reflectance product, $R_{\text{HCG}}R_{\text{HG}}$. This shows that the detection linewidth can be controlled by engineering the HCG and HG reflectances, which is feasible in the reflectance range of interest, e.g., 97 % to 99.9 %. The red circle denotes the numerically obtained linewidth of 1.1 nm (c.f. Fig. 2(d)) and reflectance product of 0.9875×0.9865 (c.f. Figs. 2(a) and 2(c)), which agrees well with the analytic relation in Fig. 2(f), while the green one represents the experimentally measured linewidth, which is discussed in the next section.

3. Fabrication and characterization

Based on the investigated design, a hybrid III-V/SOI detector sample was fabricated by heterogeneously integrating InP-based III-V layers onto an SOI wafer [13]. Firstly, Si gratings were patterned in the Si layer of an SOI wafer by using electron beam (e-beam) lithography and dry etching processes. It was followed by the direct wafer-bonding of an InP-based epitaxy wafer onto the SOI wafer and annealing at 300°C. The InP-based epitaxy wafer was grown by using our metalorganic vapor phase epitaxy (MOVPE) machine. After removing the InP substrate, InP gratings for an HCG reflector were defined in the top InP layer of the III-V layers by using e-beam lithography and dry etching processes. Then, several photo lithography, and wet and dry etching steps were performed to define mesas. After this, metal contacts were formed by using metal deposition and lift-off processes. Finally, the InP grating structure was released by sacrificially wet-etching the InGaAs layer underneath the grating layer, which forms

Optics EXPRESS

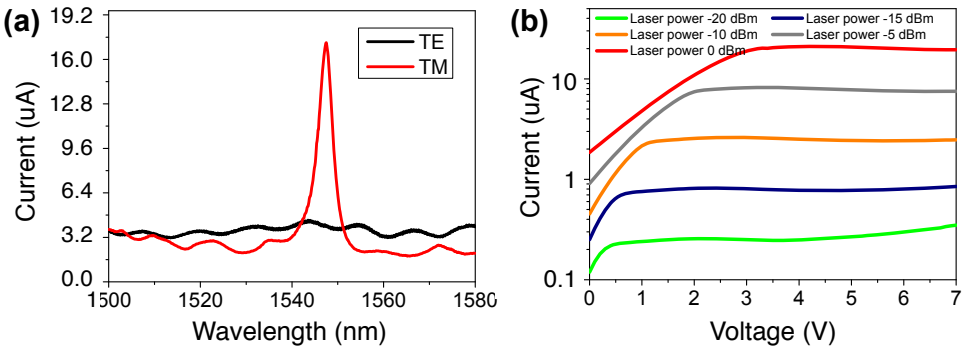

Fig. 4. (a) Measured photo-current spectra with TE and TM polarized incident lights. (b) Measured photo-current as a function of voltage at various incident light powers (TM polarization). The laser powers in the inset are readings from the tunable laser.

an HCG. An optical microscope image of the fabricated sample is shown in Fig. 3(a).

For characterizations, light from a tunable laser output was polarized and was delivered to the detector sample through a polarization-maintaining (PM) fiber, as shown in Fig. 3(b). Electrical probes that were put on the metal contacts were used to supply a bias voltage and measure the photo current. Since it is hard to directly determine the polarization of the light from the PM fiber, we accepted the polarization angle which gave the largest peak photo-current, as corresponding to the TM polarization. Then, the polarization angle which is rotated by 90° from the TM polarization angle was accepted as corresponding to the TE polarization. The power loss from the tunable laser to the end of the PM fiber is more than 10 dB.

Figure 3(c) shows the current curve as a function of reverse bias voltage, V with no incident light. The dark current in the reverse bias regime ($V > 0$) is about 0.6 nA. The differential resistance in the forward bias regime ($V < 0$) is about 450 Ω, which is attributed to the high resistance p-InP contact. This large resistance can be significantly reduced by employing a tunnel junction, which allows to replace the high resistance p-InP contact with a low-resistance n-InP contact.

Figure 4(a) shows the photo-current spectra for TE and TM polarized incident lights. The generation of photo-current is highly enhanced around 1548-nm wavelength selectively for TM polarization, which agrees with the numerical anticipation as shown in Fig. 2(d). The measured peak wavelength, λ of 1548 nm differs from the calculated one, λ_0 of 1550 nm by 2 nm, which is a small deviation in short cavity lasers. If the detection wavelength is to be more accurately controlled, a dynamic tuning by e.g., MEMS or heat is needed. The measured linewidth, $\Delta\lambda$ of about 3.2 nm is larger than the numerical anticipation of about 1.1 nm. Referring to the analytic relation plotted in Fig. 2(f), this implies that the reflectance product, $R_{\mathrm{HG}}R_{\mathrm{HCG}}$ of the fabricated sample represented by the green circle in Fig. 2(f) is smaller than the designed value represented by the red circle. This could be attributed to the deviation of the absorption coefficient of the InGaAs layer as well as layer thicknesses from the values used for simulations. Thus, for future revised devices, it is needed to experimentally measure the absorption coefficient and more carefully calibrate the growth rate through multiple growth runs, SEM measurements of thicknesses, and in-situ thickness monitoring. As discussed in [21, 33], the HG and HCG reflectances are tolerable over various typical fabrication deviations of about 10 nm. Thus, with aforementioned calibrations done, the design reflectances and linewidth will be able to be achieved.

Figure 4(b) shows the peak photo-current as a function of reverse bias voltage at several incident light powers. The photo-current increases with the bias voltage and incident power

Optics EXPRESS

increasing, and given an incident power it saturates beyond a specific voltage, which is typical for *p-i-n* PDs. In Figs. 4(a) and 4(b), we did not translate photo-currents into responsivities or quantum efficiencies, since the light receiving area, i.e., the top HCG area (12 μm$\times$12 μm) appears to be smaller than the size of the diverging incident beam from a PM fiber, at the top HCG surface. In future works, a larger device is needed for estimating responsivities.

Let us discuss the high speed potential of this RCE-PD structure. The speed of a *p-i-n* PD is determined by the transit time, τ_{TR} ($= w/v_d$) and RC constant, t_{RC} ($= (R_L + R_s)C$), where w is the depletion region width, v_d, drift velocity, R_L, external load resistance, R_s, internal series resistance, and C, internal capacitance [34]. In the current sample, approximating the depletion region width, w by the un-doped layer thickness of 386 nm and assuming a saturated drift velocity of 10^5 m/s [34], the intrinsic bandwidth, f_{in} is about 41 GHz ($= 1/2\pi t_{\mathrm{TR}}$). However, the extrinsic bandwidth f_{ex} is less than 1 GHz ($= 1/2\pi t_{\mathrm{RC}}$), mainly due to the high internal series resistance. If the resistance is reduced to e.g., 50 Ω by employing a tunnel junction, the upper cladding area is 15 μm $\times$ 15 μm, and the load resistance is small, the f_{ex} can be larger than 50 GHz. This shows that there is a potential for achieving a high speed by minimizing the parasitics in future devices.

The detection wavelength can be feasibly determined during fabrication, since the reflection phase of an HCG or an HG which influences the resonance wavelength can be controlled by changing the grating period or bar width [2, 4]. The whole C-band can be covered. This kind of control during fabrication is very limited for conventional RCE-PDs based on DBRs [35]. The same structure can be used for a laser by only changing the HG and HCG grating parameters so as to make their reflectances high enough for lasing. This implies that both a VCL and a RCE-PD can be made from the same layer structure, which enables a Si-integrated bi-directional transceiver. Furthermore, if the top HCG is actuated by using MEMS technology [8], the detection wavelength and lasing wavelength become tunable. This tuning capability will allow for accurate control of lasing and detection wavelengths, which is required for dense WDM applications.

4. Conclusion

A hybrid III-V/SOI RCE-PD has been numerically and experimentally investigated, which consists of an InP HCG, an HG with an absorbing material, and an air cavity between them. These investigations show that the field enhancement within the HG is large enough for RCE-PD operation. Numerical simulations anticipate that the proposed hybrid RCE-PD can achieve a quantum efficiency close to 100 % and a detection linewidth of about 1 nm. Characterization of fabricated samples shows that careful calibration of growth rate and absorption coefficient is required to realize them. The detection linewidth and wavelength can be feasibly engineered during fabrication by changing the reflectances and reflection phases of HCG and HG reflectors.

Acknowledgments

The author gratefully acknowledges support from the Danish Research Council through the FTP project (Grant No. 0602-01885B), the Innovation Fund Denmark through the HOT project (Grant No. 5106-00013B), as well as Villum Fonden via the NATEC Centre of Excellence.